LA-UR- 98-4288

Approved for public release; distribution is unlimited.

Title: PDM PERFORMANCE TEST RESULTS AND PRELIMINARY ANALYSIS: INCOMPRESSIBLE AND COMPRESSIBLE FLUIDS

Author(s): Donald S. Dreesen, EES-4
Eppler Gruenhagan, Consultant
John C. Cohen, Maurer Engineering Inc.
Danial W. Moran, EES-4

Submitted to: Etce '99, 75th Anniversary Conference, Feb. 1-3, 1999, Houston, TX

Los Alamos
NATIONAL LABORATORY

Form No. 836 R5
ST 2629 10/91

DISCLAIMER

PDM PERFORMANCE TEST RESULTS AND PRELIMINARY ANALYSIS: INCOMPRESSIBLE AND COMPRESSIBLE FLUIDS

Donald S. Dreesen, GeoEngineering Group, Los Alamos National Laboratory, Los Alamos, NM
Eppler Gruenhagen, Consultant, Dahlonega, GA
John C. Cohen, Maurer Engineering Inc., Houston, TX
Daniel Moran, University of Tulsa, Tulsa, OK / Los Alamos National Laboratory, Los Alamos, NM

ABSTRACT

Three, small diameter, Moineau, positive displacement (drilling) motors (PDMs) were dynamometer tested using water, air-water mist, air-water foam, and aerated water. The motors included (1) a 1.5-inch OD, single-lobe mud motor; (2) a 1.69-inch OD, 5:6 multi-lobe mud motor; and (3) a 1.75-inch OD, 5:6 multi-lobe air motor. This paper describes the test apparatus, procedures, data analysis, and results. Incompressible and compressible fluid performance are compared; linear performance, predicted by a positive displacement motor model, is identified where it occurs. Preliminary results and conclusions are (1) the performance of all three motors is accurately modeled using a two-variable, linear model for incompressible fluid and (2) the model was not successfully adapted to model compressible fluid performance.

INTRODUCTION

With the increasing acceptance and application of underbalanced drilling, compressible drilling fluids are used to transport hydraulic and pneumatic power downhole; progressing cavity PDM's are the dominant downhole motor used for underbalanced drilling (Samuel, 1997). Downhole drilling motors based on the Moineau principle (Moineau, 1930), were introduced in a single-lobe configuration in the 1950's and as multi-lobe configurations in the 1980's (Beswick and Forrest, 1982). The theoretical performance of a progressing cavity motor was described by W. Tiraspolsky (1985), and Makohl and Jurgens (1986) and mathematically detailed in a recent Ph.D. thesis (Samuel, 1997). Vetter and Wirth (1995) summarized theoretical pump performance. Incompressible performance is presented in Samuel, Miska, and Volk (1997) and compressible performance is examined in Samuel, Miska, and Li (1998). Operation of PDMs and reduced drilling performance using compressible fluids is reviewed by Graham (1995). Li, Tudor, and Cox (1997) presented PDM test data for water and multi-phase, compressible fluids.

PDM TEST PROGRAM

PDM Description. Three rotor-stator assemblies, Table 1, were assembled on a common flexible shaft and bearing assembly in a 1½-inch OD pressure housing. A 5/8-inch OD by 16-in long titanium flexible shaft connects the eccentric rotor to the concentric output shaft through the thrust and radial bearing assembly. The bearing assembly included fluid-lubricated, Teflon-impregnated-bronze journal, radial bearings rated for 500-lb_f radial load and dual tandem, fluid-lubricated, ball, thrust bearings rated for 4000-lb_f static load.

Test stand. The rotor-stator elements and common bearing section were tested on a 100-hp, rotary-disk-break dynamometer. Figure 1 is a schematic of the test setup. Three modifications to the basic water testing apparatus were made to conduct the compressible fluid tests: (1) A shroud was installed around the motor as a safety measure and to provide an annular flow path for the compressible fluid to simulate the downhole motor's heat transfer condition. (2) A 0.25-inch orifice was installed in the inlet of the swivel to apply a modest backpressure on the drilling motor to simulate a downhole pressure environment. (3) For some of the compressible fluid tests, a 0.39-inch orifice was installed in the top sub of the drilling motor to regenerate foam if insufficient mixing energy is generated or if breakdown of foam occurs in the motor-inlet flow line. The air supply included a 10-ft^3-volume tank on the compressor discharge and 80-ft of one-inch hose upstream of the air turbine meter; the inlet line included a mist and foam water injection inlet and a10-ft-long, 1-inch hose.

An eight-channel data acquisition system collected data at two samples per second. A 0.25-second filter was used to

TABLE 1 - PDM Description, Specifications, Calculated Values			
PDM Designation	#1	#2	#3
Design Fluid	Mud	Mud	Air
Lobes – rotor : stator	1:2	5:6	5:6
Stages	3	5	2
PDM Dimensions	(inches)		
Stator Housing OD / ID	1-1/2 / 1.25	1-11/16 / 1.37	1-3/4 / 1.45
Major Stator Diameter	1.172	1.106	1.190
Minor Stator Diameter	0.576	0.826	0.890
Major Rotor Diameter	0.878	0.980	1.05
Eccentricity	0.149	0.07	0.075
Pitch Length	13.33	17	24
PDM Calculated Values	Hypocycloid Envelope Profile		
Rotor Stator Interference*	Range derived from specified tolerances (inches)		
Maximum	0.011	0.035	0.027
Nominal	0.004	0.028	0.020
Minimum	**-0.003**	0.021	0.013
Cross-section area ($inch^2$)	0.343	0.197	0.228
Displacement	**f(Displacement) /Displacement^{-1}**		
Geometric Calculation	(ft-lb/psi) / (rpm/gpm)		
0.000-inch stator expansion*	0.0611 / 50.1	0.227 / 13.5	0.368 / 8.32
0.010-inch stator expansion*	0.0579 / 52.9	0.192 / 16.0	0.315 / 9.72
0.020-inch stator expansion*	0.0547 / 56.0	0.157 / 19.5	0.262 / 11.7
0.040-inch stator expansion*	0.0482 / 63.5	0.122 / 35.4	0.209 / 19.7
Water Test Slope	(ft-lb/psi) / (rpm/gpm)		
Maximum	0.0458 / 66.3	0.137 / 20.9	0.228 / 20.9
Minimum	0.0418 / 59.5	0.127 / 18.8	0.203 / 11.4
* Rotor Stator Interference is a diametrical interference, twice the actual interference.			

remove transients and noise and record smoothed steady-state data. The differential pressure across the rotor-stator is (P1-P2) for the water testing and (P0-P2) for the compressible fluid testing (Figure 1). High-data-rate acquisition to support transient motor performance analysis was conducted in parallel with the steady state data acquisition; observed pressure pulsation and motor vibration are summarized by Hamlin and Dreesen, 1999.

Water testing was conducted at four distinct flow rates between 16-gpm and 43-gpm. Torque was increased from no-load to stall with both smooth ramp tests and in discrete step tests. Air-mist, air-foam, and aerated-water tests were organized similar to the water test routine; constant-mass-flow rates were substituted for constant volumetric flow rates. Air rates ranged between 270 and 370 SCFM; water rates of ½ gpm for air-mist, 4 to 5-gpm for air-foam, and 16-gpm for aerated water were injected into the air stream. Water used in the foam and aerated water tests included 1 % Transform C foaming agent. At the inlet to the PDM the air-mist quality exceeded 97%, air-foam quality typically ranged from 75 to 93% with a few data as low as 57%, and aerated-water quality was less than 60%. No effort was made to control the quality of foam and aerated water at the rotor-stator outlet.

POSITIVE DISPLACEMENT MOTOR MODELS

For an ideal (100% efficient) positive displacement motor the rotary speed is generated by the volumetric flow. The magnitude of the speed is the flow rate divided by the displacement. Conservation of energy then requires that the motor torque equal the product of the displacement and the pressure drop across the rotor and stator elements. The actual motor speed and torque are reduced by the volumetric and mechanical efficiencies of the elements. The motor performance can be represented by a two variable linear relationship plotting the speed versus flow at a constant differential pressure and by plotting the torque versus differential pressure at constant flow.

The slope of the speed-flow plot is the inverse of the theoretical displacement (rpm/gpm). The x-intercept represents the slip (gpm) of the elements and is a measure of

TABLE 2: PDM Performance Under Compressible Fluid Power Liner Performance Model Parameters						
PDM Designation	**#1 1½ inch OD 1:2-lobe 3 Stage Mud Motor**					
Torque vs. Differential Pressure						
Fluid	**Water**	**Aerated**	**Foam**	**Foam WN**	**Mist**	**Mist WN**
Inlet Flow Rates	**41 gpm**	**NA**	**42 gpm**	**41 gpm**	**42 gpm**	**42 gpm**
Slope (ft-lb$_f$/psi)	**0.0455**		0.0405	0.0133	0.0137	0.0132
Intercept (ft-lb$_f$)	**-9.81**		-23.5	-0.580	-2.97	-2.26
R^2	**0.995**		0.374	0.288	0.300	0.482
Power vs. Differential Pressure						
R^2 for 2nd order model	**0.994**	**NA**	0.713	0.485	0.309	0.666
Rotary Speed vs. Flow						
Differential Pressures	**565 psi**	**NA**	**690 psi**	**615 psi**	**600 psi**	**575 psi**
Slope (rpm/gpm)	**59.5**		3.30	**42.0**	30.2	**47.2**
Intercept (rpm)	**-250**		+1810	**-68.3**	+223	**-226**
R^2	**0.998**		0.003	**0.770**	0.366	**0.923**
PDM Designation	**#2 1$^{11}/_{16}$ inch OD 5:6-lobe 5 Stage Mud Motor**					
Parameter (units)	**Torque vs. Differential Pressure**					
Fluid	**Water**	**Aerated**	**Foam**	**Foam WN**	**Mist**	**Mist WN**
Inlet Flow Rates	**42 gpm**	**40 gpm**	**42 gpm**	**NA**	**45 gpm**	**NA**
Slope (ft-lb$_f$/psi)	**0.130**	**0.138**	**0.152**		**0.175**	
Intercept (ft-lb$_f$)	**-57.3**	**-49.6**	**-39.1**		**-33.9**	
R^2	**0.997**	**0.839**	**0.948**		**0.822**	
Power vs. Differential Pressure						
R^2 for 2nd order model	**0.994**	0.715	**0.773**		0.373	
Rotary Speed vs. Flow						
Differential Pressures	**645 psi**	**615 psi**	**425 psi**	**NA**	**595 psi**	**NA**
Slope (rpm/gpm)	**19.0**	0.490	**16.1**		-2.99	
Intercept (rpm)	**-188**	+166	**-246**		+309	
R^2	**0.994**	0.046	**0.809**		0.008	
PDM Designation	**#3 1$^3/_4$ inch OD 5:6-lobe 2 Stage Air Motor**					
Torque vs. Differential Pressure						
Fluid	**Water**	**Aerated**	**Foam**	**Foam WN**	**Mist**	**Mist WN**
Flow Rates	**41 gpm**	**40 gpm**	**55 gpm**	**53 gpm**	**60 gpm**	**65 gpm**
Slope (ft-lb$_f$/psi)	**0.203**	**0.218**	**0.1702**	**0.2157**	**0.177**	**0.1895**
Intercept (ft-lb$_f$)	**-30.8**	**-23.7**	**-11.6**	**-16.98**	**-10.9**	**-9.80**
R^2	**0.988**	**0.868**	**0.987**	**0.984**	**0.983**	**0.961**
Power vs. Differential Pressure						
R^2 for 2nd order model	**0.969**	**0.822**	**0.838**	**0.977**	**0.858**	**0.446**
Rotary Speed vs. Flow						
Differential Pressures	**110 psi**	**175 psi**	**85 psi**	**85 psi**	**80 psi**	**110 psi**
Slope (rpm/gpm)	**11.4**	0.614	1.70	**3.52**	7.49	6.74
Intercept (rpm)	**-95.6**	+184	+335	**+254**	-21.1	-27.9
R^2	**0.971**	0.033	0.301	**0.893**	0.636	0.550

0.05-inch. This is much larger than expected based on manufacturer's specified tolerances (Table 1) and could be attributed to thermal expansion of the stator as documented in Gaynor, 1995.

Compressible Fluid Test Results. Sorted torque and speed plots for the multi-lobe air motor with several compressible fluids are compared to the motor's water powered performance on Figures 3A and 3B. Similar plots obtained for the other two motors are not shown. Linear parameters for best-fit lines for the speed and torque plots for all three motors are listed in Table 2. The backpressure nozzle was installed for all of the compressible fluid tests; the motor inlet ("foam regeneration") nozzle was installed for the tests designated with "WN" (Figure 1) and the pressure drops reported include the drop across the inlet nozzle.

Unlike the water test data plots, increased R^2 values were not consistently produced when torque data were sorted by flow and speed data were sorted by differential pressure. Less than half of the compressible fluid plots for sorted data suggest that a linear, positive displacement model will predict torque and speed as a function of flow and differential pressure. Best-fit lines with

the volumetric efficiency at the selected pressure drop. The slip is a function of the interference fit, fluid viscosity, the length of the cavity seal line, and the pressure differential. Volumetric efficiency is then (flow minus slip) / flow.

The slope of the torque-pressure plot is the theoretical displacement ($ft \cdot lb_f$/ psi) times a dimensionality constant. The x-intercept represents (in pressure) the sum of the losses in the PDM: entrance and exit pressure losses, friction, and internal viscous shearing in the elements; and motor bearing losses. The negative y-intercept shows the sum of these losses as a torque. The mechanical efficiency is then (converted torque less the sum of the losses) / converted torque.

The frictional losses are influenced by the interference fit, which is dependent on the pressure differential and the temperature. The stator element is an elastomer subject to thermal expansion greater than the expansion of metal rotor element and stator housing. The entrance losses and viscous shearing losses are dependent on the flow. If the changes in interference fit are slight and the fluid viscosity is constant, a linear model should predict motor performance for incompressible fluids.

The best-fit lines on Figures 2A and 2B are representative of commercial PDM performance. While these specific plots are not particularly useful to operators (drillers), they are the fundamental plots used to analyze positive-displacement pump and motor performance. The two-variable model based on best-fit lines through sorted performance data is assumed to be linear when the following conditions are within the modeler's required tolerances and standards. Best-fit lines through sorted data (1) exceed the required coefficient of determination, (2) have almost equal slopes and (3) intercepts that are proportional to the values of the variable being held constant. Samuel (1997) has modeled slip (leakage) as a linear function of pressure drop, two torque losses that are linear functions of speed (and flow) and pressure drop respectively, and a third torque loss that is assumed to be a constant (2^{nd} order dependency on pressure drop and speed). These losses are sufficient to realize a linear two-variable model.

The output power plot is the product of the torque and speed; where torque and speed are linear, the power plot is a 2^{nd}-order polynomial function of either variable when the complementary variable is held constant.

The x-axis intercepts generated by the linear model may not match measured no-load differential pressure and locked-rotor flow since these intercepts may occur outside the linear performance range of the motor.

DATA ANALYSIS METHODS

All ramp and step data were commingled on a single spreadsheet for the analysis. Nonlinear data for stall, near-stall, and high differential pressures were removed. Data removed included rotary speeds less than: 10 rpm for multi-lobe and 400 rpm for single lobe water testing; 100 rpm for multi-lobe and 650 rpm for single-lobe compressible fluid testing. High pressure drops removed were greater than: 1400 psi for the single-lobe mud motor, 2330 psi for the multi-lobe mud motor, and 700 psi for multi-lobe air motor. The remaining data were then sorted to generate: (1) **torque versus differential pressure** plots at selected inlet-flow rates; (2) **rotary speed versus flow** plots at selected differential pressures; and (3) **output power versus differential pressure** plots calculated for a normalized flow rate. Flow rates and differential pressures for plotting were chosen using histograms to identify values with abundant data.

Linear best-fit lines and their characteristic parameters, slope, intercept, and coefficient of determination (R^2) were calculated for the torque and rotary speed plots. The 2^{nd}-order polynomial best-fit curves and R^2 were calculated for the power plots. R^2 greater than 0.75 is assumed to be indicative of linear performance; R^2 greater than 0.95 is assumed to be linear or 2^{nd}-order polynomial performance for power. The R^2 values for the sorted data subsets were compared to R^2 values for the unsorted data to determine where a 2-variable linear model is justified over a single variable model with a constant offset.

RESULTS

Incompressible Fluid Test Results. Water powered torque and speed plots for the multi-lobe **air** motor, ***Motor #3,*** are shown on Figures 2A and 2B. Similar plots for the other motors are not shown. The maximum and minimum slopes of best-fit lines for the torque and speed plots are listed at the bottom of Table 1.

R^2 coefficients for the best-fit lines for commingled **torque** versus pressure drop data are 0.916 for the air motor and 0.976 and 0.983 for the mud motors. Sorting by flow rate increases the minimum R^2 above 0.95 for the mud motors and for two of the four flow rates for the air motor. Sorted data produces best-fit lines with a series of x-intercepts that increase with the flow rate. No-load and loaded motor performance up to a near stall is modeled accurately with a linear, two-variable model.

R^2 coefficients for best-fit curves of commingled rotary **speed** versus flow data range from 0.196 to 0.966; sorting by differential pressure increases the minimum R^2 to 0.977 for the three motors and the expected linear relationship is verified for sorted data. Sorted data produces best-fit lines with x-intercepts that increase with the differential pressure. The x-intercepts are distinctly different from the actual data near stall. Except under near stall conditions, motor performance is predicted accurately with a linear, two-variable model.

To calculate motor displacements consistent with water test data (slopes shown at the bottom of Table 1), large rotor-stator (diametrical) interference must be assumed: 0.03-inch to

R^2 greater than 0.75 are shown in **bold** on Table 2. Where linear performance is indicated, the R^2 values for compressible fluids are not high enough to be definitive. With one exception, all y-axis intercepts for the potentially linear, sorted data plots are negative and x-axis intercepts are therefore positive and imply losses (as opposed to sources).

Motor #1. None of the torque plots and only two rotary speed plots, the air-mist (WN) and air-foam (WN), show possible linear performance for the single-lobe, mud motor; plots for data without the inlet nozzle have very low R^2 values. The slopes of the two (indicated linear) speed plots are lower than the slope for water and the motor's inverse displacement; increased slip flow and stator contraction with or without the formation of a rotor-stator gap are plausible explanations.

Motor #2. No tests were run with the **inlet** flow nozzle installed. All of the torque plots for the multi-lobe mud motor indicate possible linear performance and have positive x-axis intercepts. The slopes of the best-fit torque lines are higher than the slopes for the water test data but within the calculated displacement range for 0.015 to 0.03-inch interference. The rotary speed plot for air-foam has an R^2 of 0.809. This is the only case for the data presently analyzed where simultaneous linear torque and rotary speed performance is indicated. It also has a positive x-axis intercept and a displacement slope within the calculated inverse displacement range for the 0.01-0.02-inch interference.

Motor #3. All of the torque plots for the multi-lobe air motor indicate possible linear performance and have positive x-axis intercepts. The slopes of the best-fit lines are within the range of or lower than slopes for the water test data and consistent with the inverse displacement for an interference of 0.04-inches. The rotary speed plot for air-foam with the foam-regenerating nozzle has an R^2 of 0.893; however its slope is inconsistent with a linear model because it produces a positive y-axis intercept. Steady state, positive no-flow motor speed is viable in pump (compressor) mode but not in motor operation. Rotary speed plots for aerated water and air foam without the nozzle also have positive intercepts but have very low R^2 values.

Rotary Power Output. Calculated power plots for each motor are shown on Figures 4A, 4B, and 4C. The output power is the product of the torque and speed normalized to a common flow rate by multiplying by the volumetric flow divided by the water test flow. Sorted data for each of the several compressible fluids and (the torque plot) flow rates were used to produce the power plots. The R^2 values for a best-fit 2^{nd}-order polynomial curve are listed in Table 2.

At a given differential pressure and at similar flow rates, the multi-lobe motors produce more power with compressible fluids than with water. However the maximum power using compressible fluids was severely limited because the differential pressure developed across the motors is very low. The single-lobe motor operates at a much more reasonable differential pressure level but produces only 1/3 the waterpower with compressible fluids.

There is no consistent trend among the three motors with regard to the power conversion based on fluid type. Air mist and air foam produce higher power than aerated water but foam did not produce consistently higher power than mist.

The insertion of the upstream foam re-generation nozzle in the multi-lobe air motor increased the power conversion with air-mist and air-foam slightly but decreased the aerated-water power. In the single-lobe motor the nozzle did not consistently increase the maximum power output but did improve the lower differential pressure performance significantly.

DISCUSSION OF RESULTS

Two-variable, linear model. Sorting of water powered performance data to produce constant-flow-rate plots for the torque versus pressure and constant-differential-pressure plots for the speed versus flow plots increases or at least maintains already high R^2 values. Sorting of compressible fluid data produces no consistent increase in R^2. A two-variable, linear model based on inlet volumetric flow and differential pressure is appropriate for the water performance data but is not applicable for compressible fluid performance. Attempts to use some of the dimensionless variables proposed by Samuel (1997) to model compressible fluid performance have not, to date, produced plots with higher, best-fit-line, R^2 values than obtained with inlet volumetric flow and differential pressure. Plots based on calculated (adiabatic isentropic expansion) volumetric flow rates within the rotor-stator elements also have failed to produce a better correlation.

Locked-rotor flow predicted by a linear rotary speed versus flow model increases with the differential pressure of an incompressible fluid. No similar trend was observed in the compressible fluid data.

The no-load differential pressure predicted by a linear torque versus pressure drop model for the water data increases with the inlet flow rate. No similar trend was observed in the compressible fluid data.

Loss Elements. The slope of the torque versus pressure plots is less than the calculated displacement even when a 0.02-inch stator expansion is assumed for the calculation. The difference between the inverse of the speed plot slope and the torque slope is consistent with a two-variable, linear model for incompressible fluids and the loss elements proposed by Samuel (1997). Slopes for some of the air data suggest negative loss elements or sources. This supports other evidence that suggests a two-variable, linear model based on flow and differential pressure is not valid for compressible fluids.

Compressible Fluid Performance. Under compressible fluid power the multi-lobe air motor design is more efficient than the multi-lobe mud motor. The limited differential pressure across the air motor limits the maximum power output to less than 1/3 the maximum power with water. For compressible fluids, the slopes of the best-fit lines for the sorted, rotary speed versus flow data are less than the slopes for the sorted water

data. They are sometimes less than the calculated inverse displacement. The difference could be the result of (1) contraction of the rubber stator due to substantial cooling from air expansion or (2) power fluid expansion in the inter-stages creating a rotor speed based on a higher flow rate than the inlet flow. Since substantial cooling was not evident in the testing, multi-lobe motors appear to be able to extract some of the energy released in the expansion of the air as well as the displacement energy. The single-lobe motor is apparently very inefficient in extracting even the displacement energy from the air stream.

Inlet Nozzle. The pressure drop measured included the drop across the nozzle; thus the nozzle represents an additional loss. Since the improvement occurred for both the air-mist and the air-foam fluids, it is unlikely that foam re-generation explains the increased power output with the inlet nozzle, where it was observed. There is some indication that motor performance may be stabilized with the use of an inlet nozzle. The slow response of PDMs with compressible power fluids to changes in torque was recognized by Graham (1995) to be a significant factor in the stalling and runaway tendencies observed. Fluid compression or expansion in the large-volume drill-stem delays the required differential pressure adjustments. The inlet nozzle can be used to reduce the volume of the effective inlet chamber by several orders of magnitude. There is some evidence to support this use of an inlet nozzle in the power curve plots but it is not conclusive. The nozzle was sized for foam generation and was probably too large for a definitive evaluation of stability enhancement of motor performance.

CONCLUSIONS

1. Incompressible power fluid performance is accurately modeled for the three motors tested with a simple, two-variable, linear model. The constants for the model are readily determined from the slopes and extrapolated intercepts on the torque and speed plots of water performance data. The model is reasonably accurate from no-load to full load but is not accurate in a near stall condition. The model is not readily adapted to predict performance of these motors under compressible fluid power.
2. The multi-lobe air motor design extracts significantly more power from a low-pressure air stream than the multi-lobe mud motor design.
3. The single-lobe mud motor develops a higher-pressure drop across the rotor stator unit than the multi-lobe motors but the pressure drop is apparently dissipated and not converted to torque.
4. The insertion of a small diameter nozzle upstream of the rotor stator unit appears to increase the efficiency of the air motor under air-foam and air-mist power. Its benefit may be due to improved motor response to torque changes but it does not appear to be related to foam regeneration.

ACKNOWLEDGEMENTS

The work documented in this report was funded by the U.S. Department of Energy sponsored Natural Gas and Oil Technology Partnership through a contract with the University of California, Los Alamos National Laboratory. The GeoEngineering Group directed the work in the Earth and Environmental Sciences Division at the Laboratory. Roper Pump Company produced the rotor-stator units tested and Roper, in support of this project, donated the tooling cost required to fabricate the air-motor design. The motor testing described was performed at the Drilling Research Center at Maurer Engineering Inc.

REFERENCES

Beswick, A.J. and J. Forrest, 1982, "New Low-Speed High-Torque Motor Experience in Europe," SPE 11168, SPE ATC&E, New Orleans, LA, Sept. 26-29.

Hamlin, D.B. and D.S. Dreesen, 1999, "Analysis of Vibration and Pressure Pulsation in Positive Displacement Drilling Motors," in preparation for the 1999 Energy Sources Technology Conference & Exhibition (ETCE '99), February 1-3, Houston, TX.

Gaynor, T.M., 1995, "Severe Environment Turbine Powered Steerable Motors," PD-Vol. 65, Drilling Technology, ASME, pp. 273-283.

Li, J., R. Tudor, and R. Cox, 1997, "Positive Displacement Motor Test with Two-phase Flow," SPE 38425, 2nd N. American Coiled Tubing Round Table, Mongomery, TX, April 1-3.

Moineau, R.L.J., "Gear Mechanism, 1932, " United States Patent No. 1,892,217, Dec. 27, 1932.

Makohl, F. and R. Jurgens, 1986, "Evolution and Differences of Directional and High-Performance Downhole Motors,' IADC/SPE 14742, 1986 IADC/SPE Drilling Conference, Dallas, TX, February 10-12, pp. 189-196.

Samuel, G.R., 1997, "Mathematical Modeling and Design Analysis of the Power Section of a Positive Displacement Motor (PDM)," Ph.D. Dissertation, Department of Petroleum Engineering, The University of Tulsa.

Samuel, G.R., S. Miska, and L. Volk, 1997, "Analytical Study of the Performance of Positive Displacement Motor (PDM)," SPE 39026, 5th Latin and Caribbean Petroleum Conference and Exhibition, Rio de Janeiro, Brazil, August 30 – Sept. 3.

Samuel, G.R., S. Miska, and J. Li, 1998, "Performance Index Provides Engineers with Tool to Select PDM, Track Performance," Oil and Gas Journal, Vol. 96, No. 35, August 31, pp. 59-63.

Tiraspolsky, W. 1985 "Hydraulic Downhole Drilling Motors," Gulf Publishing Co.

Vetter, G. and W. Wirth, 1995, "Understanding Progressing Cavity Pump Characteristics and Avoid Abrasive Wear," Proceedings of the Twelfth International Pump Users Symposium.

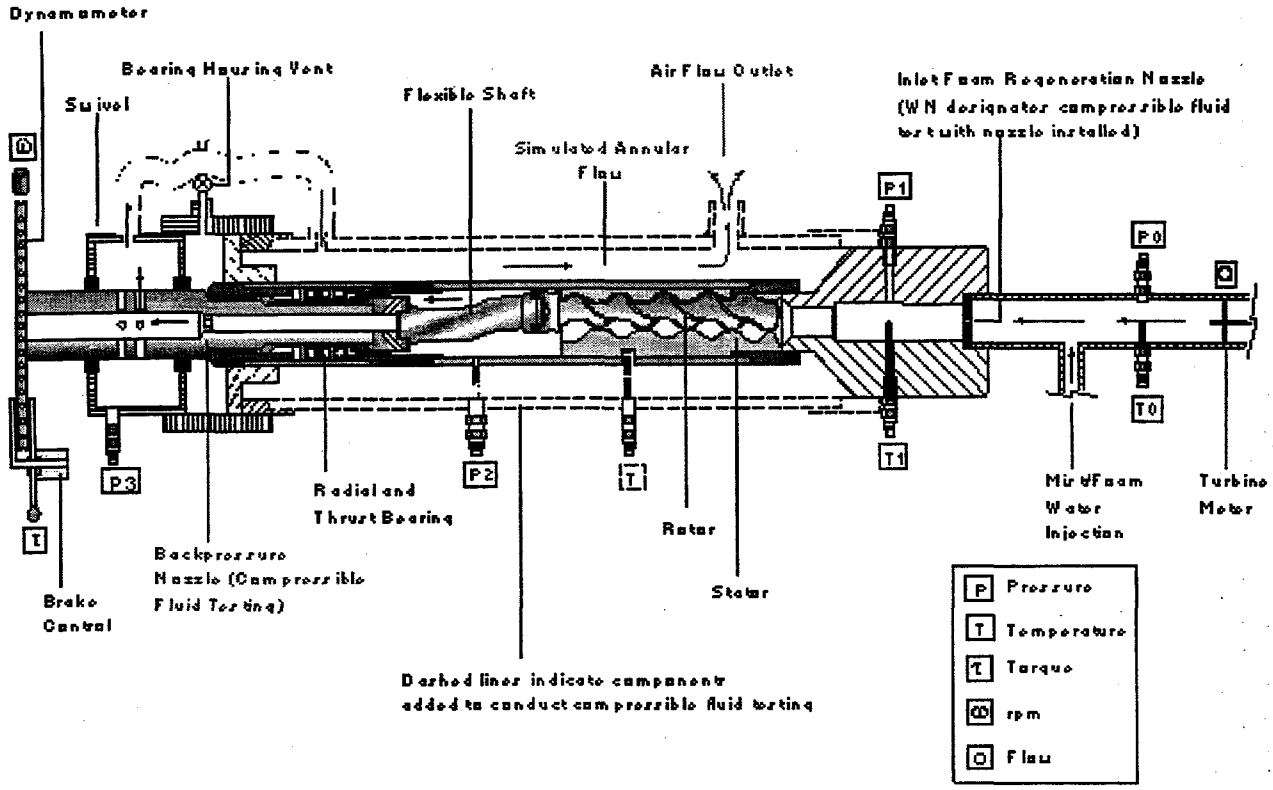

Figure 1. Schematic of the Test Apparatus.

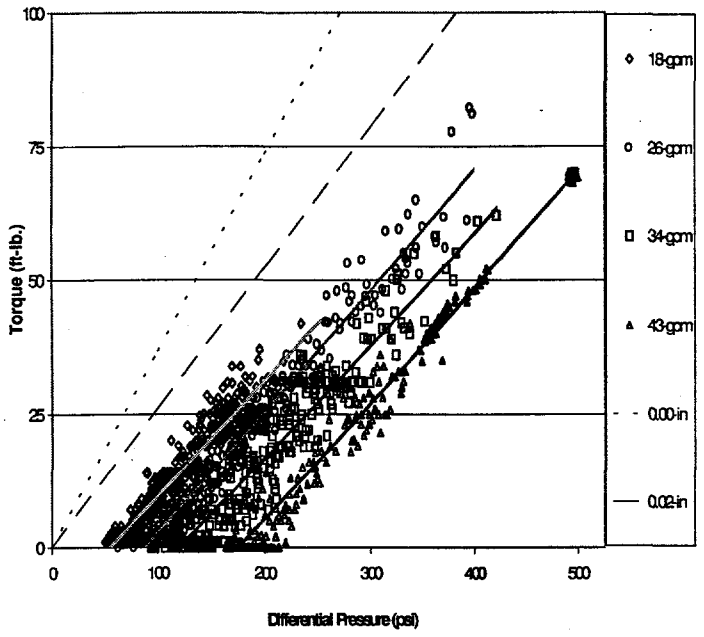

A. Torque vs. pressure drop for flow rates shown. Calculated displacement for rotor interference.

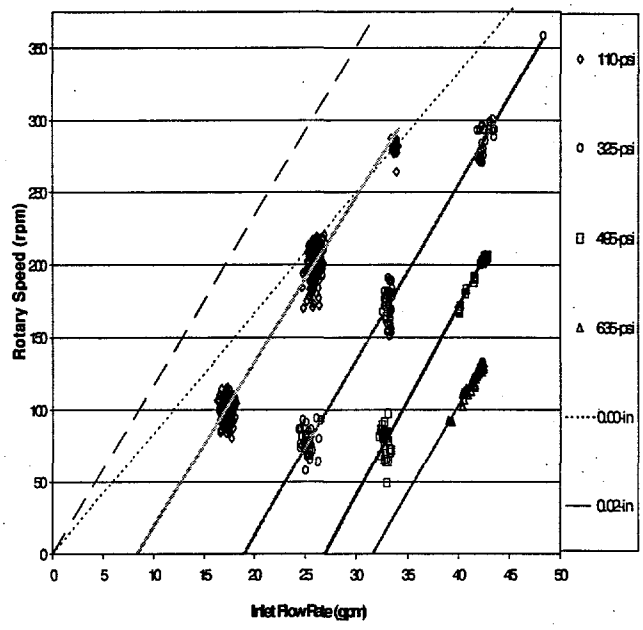

B. Rotary speed vs. flow for pressure drops shown. Calculated (displacement^{-1}) for rotor interference.

Figure 2. Water test results for *Motor #3* (13/4-inch OD, 5:6 multi-lobe, 2-stage, air motor)

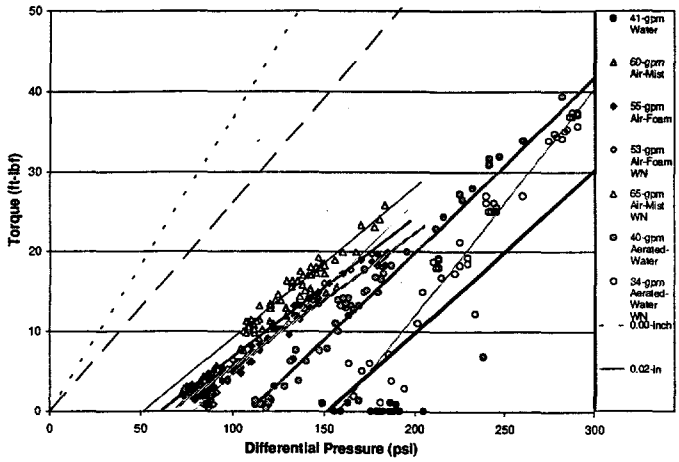

A. Torque vs. pressure drop for rates and fluid shown. Calculated displacement for rotor interference.

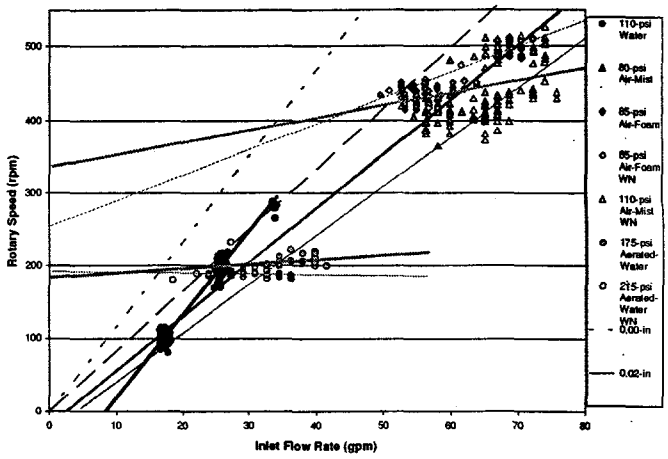

B. Speed vs. flow for pressure drop and fluids shown. Calculated (displacement^{-1}) for rotor interference.

Figure 3. Compressible fluid and water test results for *Motor #3.* (13/4-inch OD, 5:6 multi-lobe, 2-stage, air motor)

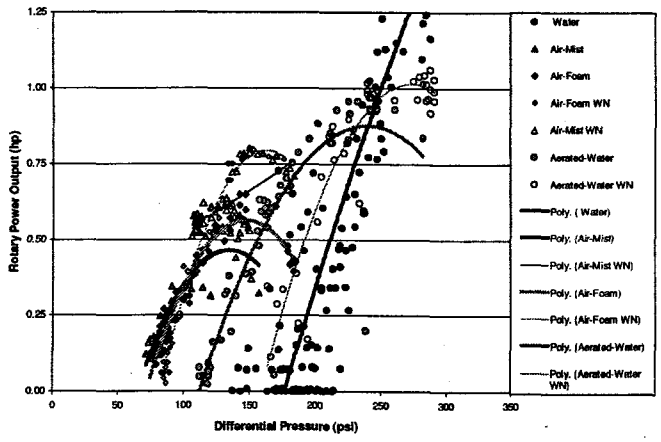

A. *Motor #3.*
(13/4-inch OD, 5:6 multi-lobe, 2-stage, air motor)

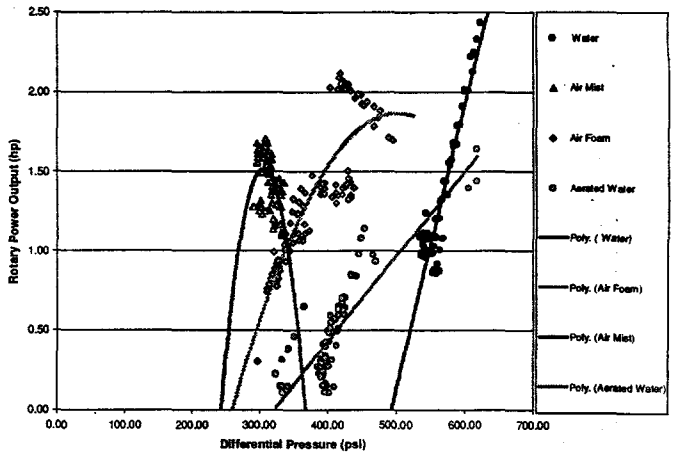

B. *Motor #2.*
(111/16-inch OD, 5:6 multi-lobe, 5-stage, mud motor)

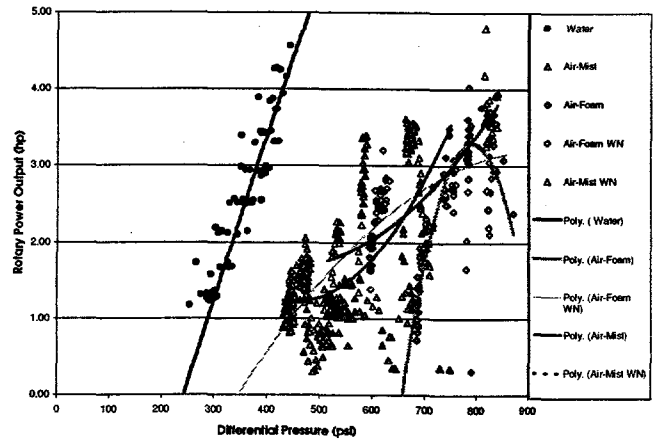

C. *Motor #1.*
(11/2-inch OD, 1:2 single-lobe, 2-stage, air motor)

Figure 4. Output power for compressible fluids and water.